Separation and Characterization of Double-Wall Carbon Nanotube Subpopulations

ARTICLE *in* THE JOURNAL OF PHYSICAL CHEMISTRY C · JUNE 2010

Impact Factor: 4.77 · DOI: 10.1021/jp9110376

Separation and Characterization of Double-Wall Carbon Nanotube Subpopulations

Ji Yeon Huh,[†] Angela R. Hight Walker,[‡] Hyun Wook Ro,[†] Jan Obrzut,[†] Elisabeth Mansfield,[§] Roy Geiss,[§] and Jeffrey A. Fagan*[,†]

[†] *Polymers Division,* [‡] *Physics Laboratory, National Institute of Standards and Technology, Gaithersburg, Maryland 20899,* [§] *Materials Reliability Division, National Institute of Standards and Technology, Boulder, Colorado 80305*

Received: November 20, 2009; Revised Manuscript Received: May 13, 2010

Surfactant-encapsulated double-wall carbon nanotubes (DWCNTs) synthesized by the high-pressure carbon monoxide decomposition (HiPco) process were separated by length and electronic characteristics using density gradient ultracentrifugation (DGU). To ensure our study focuses only on the behavior of DWCNTs, dispersed DWCNTs were first isolated following the method of Green et al. [Green, A. A.; Hersam, M. C. *Nat. Nanotechnol.* **2008**, *264*, 1], utilizing the differences in buoyant density of DWCNTs from that of impurity single-wall carbon nanotubes (SWCNTs) and multiwall carbon nanotubes contained in the parent soot. By increasing the density difference between the nanotubes and the density gradient medium, we exploited the length-dependent translation of the nanotubes in response to applied centrifugation to isolate narrow length distribution DWCNT fractions. The length-dependent intrinsic optical response of DWCNTs is consistent compared with the previously reported values for SWCNTs. The controlled addition of cosurfactants is shown to allow resolution of DWCNTs by electronic structure, as demonstrated through optical absorbance, Raman spectra, and electrical conductivity measurements. Measurements of conducting films prepared from separated fractions exhibit significant property differences in the enriched materials.

Introduction

Double-wall carbon nanotubes (DWCNTs), consisting of two concentric graphene cylinders, are the first multiwall carbon nanotube (MWCNT) allotropes, and exist in an intermediate regime with other few-walled nanotubes between single-wall carbon nanotubes (SWCNTs) and, typically, much larger diameter MWCNTs. Because of their small diameters (typically $d \leq 2$ nm), many DWCNTs have been shown to have properties similar to those of SWCNTs, enabling their use in enhancing the spatial resolution of sensors and as field enhancement for electron emitters.[2−6] However, it has also been predicted that DWCNTs should exhibit enhanced mechanical and electrical properties relative to SWCNTs and MWCNTs.[6,37−46] Because these factors play a critical role in various thin film applications,[3−5] the commercial market for DWCNT materials will likely grow at the expense of SWCNTs and MWCNTs in the future. In addition, DWCNTs are ideal for studying the intrinsic interaction and coupling behaviors between concentric graphene cylinders, as they are the simplest form of MWCNTs.[6,47,48] Current methods of synthesizing DWCNTs, however, also produce significant amounts of SWCNTs, MWCNTs, and carbonaceous impurities, which have led to inconsistency in the measured properties for DWCNT samples, and restricted their development for device applications. To realize optimal performance in high value applications, it is important to develop techniques to prepare monodisperse DWCNT populations with uniform physical and electronic structures.

Potential applications of carbon nanotubes depend on their unique electronic structure, which arises from the quantization of the electronic wave vector of the one-dimensional system through the rolling of a graphene plane into a cylinder, forming the nanotube. The chiral vector in units of hexagonal elements connects two points on this plane, defining the nanotube chirality in terms of two integers, n and m.[7] When $|n - m| = 3q$, where q is an integer, the nantoube is metallic or semimetallic, while remaining species are semiconducting with a geometry-dependent band gap. Arnold et al.[8] demonstrated that it was possible to separate a mixed population of SWCNTs into fractions predominantly of a single electronic type, characterized as either metallic or semiconducting, through the use of competing mixtures of surfactants and density gradient ultracentrifugation (DGU). Empirically, the different adsorption of the surfactants onto nanotubes with different electronic type alters the buoyancy of one or both of the species, enabling separation. The organization of the surfactant, based on the energetic balance among nanotubes, surfactants, and water, is hypothesized to determine the metal-semiconductor selectivity. Yanagi et al.[9] demonstrated that SWCNTs with a single electronic type can display various colors depending on their electronic types and average diameters due to different chirality distributions. Since DWCNTs are constructed from two SWCNTs, both inner and outer walls can have different chiralities, and are thus both more complicated structures than SWCNTs and potentially useful for additional applications. For instance, DWCNTs with metallic layers may be useful for coaxial cables or capacitors. Other combinations of electronic types of the inner and outer walls are better suited for applications such as field emission transistors and biosensors.[3−5,40−46] Hayashi et al.[10] reported that it is possible to passivate the outer walls, leaving the inner wall optically active through a fluorination process. The inner wall is then protected from interacting with other substances, which may be a requirement for nanotube-based integrated circuits.

The length of the carbon nanotubes after processing is the other key property that dramatically impacts the wide range of potential applications for these materials. Although their cylindrical diameters are typically on the order of nanometers, lengths

* Corresponding author. E-mail: jeffrey.fagan@nist.gov.

10.1021/jp9110376
Published on Web 06/10/2010

can be up to several micrometers or more. Generally longer lengths are desired to reduce percolation thresholds, although some applications require short materials. Due to their high aspect ratio, a carbon nanotube is also a prototype one-dimensional system that has a quantized electronic density of states in the form of van Hove singularities similar to molecular systems.[11] In order to sort the carbon nanotubes by length, several chromatographic techniques have been developed such as gel electrophoresis and size exclusion chromatography (SEC).[12−14] These techniques can produce well-defined length distributions; however, particularly for SEC, the separated length range is typically limited to less than 600 nm due to the exclusion limit of the column stationary phase. Recently, the fractionation of longer length SWCNTs in excess of 1 μm was achieved by exploiting the length-dependent friction coefficient of the SWCNTs through a dense liquid as driven by ultracentrifugation.[15,16] An additional benefit of this technique is the use of a similar experimental design to DGU, with the key difference being that the length separation is dominated by transient motion, whereas DGU separations are driven by buoyancy equilibrium. Both DGU and centrifuge-based length separations have been shown to be well suited for production of milligram-to gram-scale SWCNT fractions with various ranges of length and diameter, based on noncovalent, reversible surfactant chemistry. Recent reports have highlighted the length-dependent properties of SWCNTs, including the intrinsic optical response of SWCNTs,[17] the cellular uptake of DNA-wrapped SWCNTs,[18] and the conductivity of thin SWNT networks.[19] For many applications, increasing the length of the nanotube as much as possible results in the best combination of material properties. In the case of DWCNTs, their average length was found to be longer than SWCNTs, although an identical sonication condition was applied to disperse both of them in the surfactant solution.[1] This suggests that DWCNTs are likely to be more resistant to a sonication-induced cutting effect due to their improved mechanical properties, and thus may yield higher amounts of longer fractions after solution processing.

In this work, we report on the separation of surfactant-encapsulated DWCNTs by length and metallic property using DGU. Starting with a batch of commercial DWCNT soot, we followed the experimental approach of Green et al.[1] to separate the various components in the raw soot, including SWCNTs, DWCNTs, MWCNTs, and impurities, to achieve a primarily DWCNT separation. DWCNTs were separated by length, demonstrating that centrifugation methods developed for SWCNTs can be used to isolate distinct DWCNT length fractions that will allow for length-dependent property characterization. We then demonstrate the optimization of metal−semiconductor separation of DWCNTs using the controlled addition of cosurfactants, which was correlated to ultraviolet−visible−near-infrared (UV−vis−NIR) optical absorbance, Raman spectra, and electrical conductivity. Finally, we conclude with the implications and the future directions of this work.

Experimental Section[49]

DWCNTs in this work were isolated by a three-step process. First, as-produced starting materials (Unidym, Inc., Lot # DW 426VA), synthesized by the high-pressure carbon monoxide decomposition (HiPco) process were added 1 mg/mL in a 2% by mass per volume sodium deoxycholate solution (DOC, Sigma). This suspension was immersed in an ice water bath, and sonicated with a 0.64 cm probe-tip sonicator (Thomas Scientific) at 27 W for 1 h. Each suspension was then centrifuged in a JA-20 fixed angle rotor (Beckman Coulter) at 35000*g* and 10 °C for 2 h. After centrifugation, the initial suspension was separated into a liquid supernatant, primarily containing individualized carbon nanotubes and a solid pellet on the bottom, which contains metallic and carbonaceous impurities. This centrifugation step is hypothesized to remove most non-nanotube impurities; however, the supernatant still contains a mixed nanotube dispersion with orthogonal distributions of different diameters, number of the walls, lengths, and chiralities.

Green et al.[1] demonstrated that the different components of the mixed nanotube dispersion remaining after this initial centrifugation could be separated by the number of walls using DGU. Following their report, density gradients were created by layering a density modifier, iodixanol, purchased as OptiPrep (5,5′-[(2-hydroxy-1-3-propanediyl)-bis(acetylamino)]-bis-[*N*,*N*′-bis(2,3dihydroxylpropyl-2,4,6-triiodo-1,3-benzenecarboxamide]) (Sigma-Aldrich), ranging from 20 to 40% in centrifuge tubes. Aliquots of the mixed nanotube dispersion were loaded at the top of density gradients; this prevents the SWCNTs from reaching or passing through the isopycnic point of the desired DWCNT layer. DOC concentration was kept as 2% in all layers, ensuring no concentration gradient. Purification of DWCNTs was carried out both in a fixed angle (90°) VTi 65.2 rotor (Beckman-Coulter) at 20 °C and 385000*g* for 1 h or in a swinging bucket SW.32 Ti rotor (Beckman-Coulter) at 20 °C and 126000*g* for 19 h with comparable results. After the separation, each fraction was collected by hand pipetting from the top.

For length separation experiments, a modified version of the protocol in refs 15 and 16 was used. Density gradients were created by layering 1 mL of 40% (1.21 g/mL), 1 mL of 30% iodixanol (1.16 g/mL) containing the DWCNTs, and 20 mL of 26% (1.14 g/mL) iodixanol in centrifuge tubes. Note that this density is substantially greater than the average density of the dispersed DWCNTs (∼1.11 g/mL). All layers contained 1% DOC. Centrifugation was typically carried out in a swinging bucket SW.32 Ti rotor at 4 °C and 34000*g* for 49 h. After the separation, individual fractions were collected by hand pipetting from the top in 0.75 mL increments.

In electronic type separation experiments, protocols were adapted from refs 8 and 9. Density gradients were created by layering 1 mL of 40% (1.21 g/mL) and 2 mL of 32% (1.17 g/mL) iodixanol containing the DWCNTs, and 20 mL of 30% iodixanol (1.16 mg/mL) in centrifuge tubes. The concentration of surfactants were 1.25% sodium dodecyl sulfate (SDS, Sigma) and 1.25% sodium cholate (SC, Sigma) in the top layer, 1% SDS and 0.5% DOC in the DWNT injection layer, and 0.75% SDS and 0.75% SC in the bottom layer. Centrifugation was typically carried out in a swinging bucket SW.32 Ti rotor at 20 °C and 126000*g* for 19 h. Fractions were collected by hand pipetting from the top.

UV−vis−NIR experiments were made in transmission geometry on a PerkinElmer Lambda 950 UV−vis−NIR spectrophotometer over a wavelength range of 2500−185 nm. The incident light was circularly polarized prior to the sample compartment, and the spectra were corrected for both dark current and background. The optical absorption spectra were recorded at 1 nm increments with an instrument integration time of at least 0.16 s per increment using a 2 or 10 mm path length quartz cuvette. The reference beam was left unobstructed, and the subtraction of the appropriate reference sample was performed during data reduction. For some samples, an ultrafiltration cell (Millipore 8003, 8010, or 8050) was used to reduce or remove the iodixanol concentration or to concentrate the

nanotubes prior to measurement;[15,16] this allows for increased signal-to-noise ratio for measurement of absorbance at UV wavelengths shorter than 320 nm.

Dynamic light scattering (DLS) was performed in the VH scattering mode (crossed polarizers) with an argon ion (Ar+) laser ($\lambda = 532$ nm) at 25 °C using a Brookhaven Instruments BI-200SM. The correlation functions were measured at a minimum of five different angles at each sample with a minimum of five repetitions at each angle. At each angle, the rotational relaxation time was obtained by fitting the correlation function to an exponential function, and the extrapolated intercept at zero scattering vector for the inverse rotational relaxation time was related to the rotational diffusion constant, D_r. Lengths were then calculated by comparing the measured rotational diffusion constant with the established theoretical expression for a thin rigid rod, $D_r = 3k_BT\{[\ln(L/2r) - 0.8]/\pi\eta L^3\}$, where L is the tube length, r is the tube radius, and η is the viscosity of solvent.[20,21]

The scanning electron microscopy (SEM) images of the deposited nanotube networks were obtained using a Hitachi S4700 field emission scanning electron microscope.

All samples were prepared for analysis in the transmission electron microscope (TEM) by depositing diluting the surfactant to ~0.25% in ultrapure water. Small drops (~30 μL) of suspended DWCNTs were then deposited onto a thin holey carbon TEM grid using a micropipet. The drop was allowed to dry completely. The grid was then mounted in a single-tilt sample holder for TEM observation. All images presented here were taken at 200 keV under low-dose operating conditions in the TEM. Low dose means that the electron flux onto the samples was restricted with a small condenser aperture (typically 40 μm in diameter) and underfocusing the illumination to the minimum that would allow an image to be captured with a 2 s exposure. All images were captured by use of a 1 MP charge-coupled device (CCD) camera located below the viewing chamber. Most were captured at a TEM optical magnification of 300 kX with the objective lens at or near the Scherzer defocus condition, which in our microscope is 76 nm.

Raman spectra were collected in a collinear 180° backscattering configuration. An Ar+ laser (Coherent Innova Sabre with multiline visible head) provided the 514.5 nm excitation; approximately 20 mW of power was focused to a spot size of approximately 100 μm within the liquid sample volume. Samples were measured in a glass vial that was held immobile for all of the measurements. The spontaneous Raman backscattered light was collected with a triple grating spectrometer (Dilor XY800) and a liquid nitrogen cooled CCD detector. The integration time for the DWCNT fractions was 90 s averaged over four scans, which was an appropriate time to obtain a signal-to-noise ratio greater than 50. Data were collected with excitation at (514.5, 632, and 785) nm. Raman frequency shifts in the range from (50 to 400) cm^{-1} were measured, covering the region of spectral shift in which radial breathing modes (RBMs) are observed. Data was scaled for the incident laser intensity and adjusted by the subtraction of a small consistent background signal, generally less than a few percent of the feature intensity.

NIR fluorescence spectra were measured using a Horiba Jobin Yvon nanolog-3 spectrofluorometer with a liquid nitrogen cooled InGaAs array detector and a 450 W xenon lamp. To account for differences in concentration, fractions were diluted to a common absorbance of ~0.05/cm at 775 nm, and were measured in a 10 mm square quartz cuvette.

Tapping-mode atomic force microscopy (AFM) measurements were conducted using a Nanoscope IV system (Digital Instruments) operated under ambient conditions with standard silicon tips (NanoWorld, Si Probes; 225 μm length; normal spring constant, 48 N/m; resonance frequency, 190 kHz). Individual length-sorted DWCNTs were deposited on Si-wafers with a (3-aminopropyl)triethoxysilane (APTES, Sigma-Aldrich) self-assembled monolayer (SAM) as described in ref 1. Lengths of nonoverlapping and identifiable DWCNTs were counted within the Nanoscope software.

Thin films of nanotubes were prepared using a vacuum filtration process[22] by dispersing a solvent onto the porous cellulose ester membrane, diameter of 47 mm with 50 nm diameter pore (Millipore). The purified and sorted nanotube solution was diluted with deionized (DI) water and deposited on the membrane using a micropipet. The low nanotube concentration in each fraction precluded an absolute determination of nanotube concentration by direct weighing. Instead, the mass of nanotubes deposited on the membrane was estimated by comparing with the UV−vis−NIR absorbance of a sample with known concentration. To wash away the remaining surfactant in a nanotube solution, the deposited nanotubes were vacuum filtered with 40 mL of a mixture of isopropanol and DI water (1:4 by volume). The DWCNT membranes were then dried overnight at 40 °C. The optical characteristics of the carbon nanotube films obtained by the vacuum filtration were determined by measuring the diffuse optical reflectance in the wavelength range of 300−1800 nm, using a diffuse reflectance accessory kit for the Lambda 950. The reflectance spectra were normalized to the reflectivity of the filter membrane without DWCNTs, which we used as a nonabsorbing reference. Thus, the spectra primarily represent the wavelength-dependent transmittance of the film.[19]

To measure the electrical characteristics of the network films, an interdigitated gold electrode pattern was deposited directly on top through a shadow mask.[19] Electrical measurements were analyzed in terms of complex impedance, yielding the impedance magnitude (|Z*|) and the corresponding phase angle (θ) over the frequency range of 40 Hz to 10 MHz by using a four-terminal fixture attached to an Agilent 4294A precision impedance analyzer. The impedance analyzer was calibrated with a standard extension adapter to short, load, and open standards. The real part (σ') of the complex sheet (surface) conductivity was determined from the measured impedance normalized by the geometry of the electrode pattern, $\sigma' = l/[|Z|\cos(\theta) \times d]$ in units of $(\Omega/\text{square})^{-1}$ or Siemens-square (S-square). Here, l is the total length of the finger electrodes, and d is the distance between the fingers. In our measurements, $l = 9$ cm and $d = 800$ μm. The thickness of the deposited gold electrodes was approximately 0.1 μm. The lowest measurable sheet conductivity in our system was $\sigma' \approx 5 \times 10^{-12}$ S-square at 100 Hz. The sheet conductivity of dried blank membrane substrates without carbon nanotubes was typically below 10^{-11} S-square at 100 Hz. The combined relative experimental uncertainty of the measured conductivity magnitude was within 4%, while the experimental uncertainty of the phase angle measurements was about ±0.5°.

Unless stated otherwise, the standard uncertainty throughout this contribution is denoted by error bars equal to one standard deviation.

Results and Discussion

As shown in Figure 1a, four sets of bands with different buoyant densities were typically obtained from DGU separation

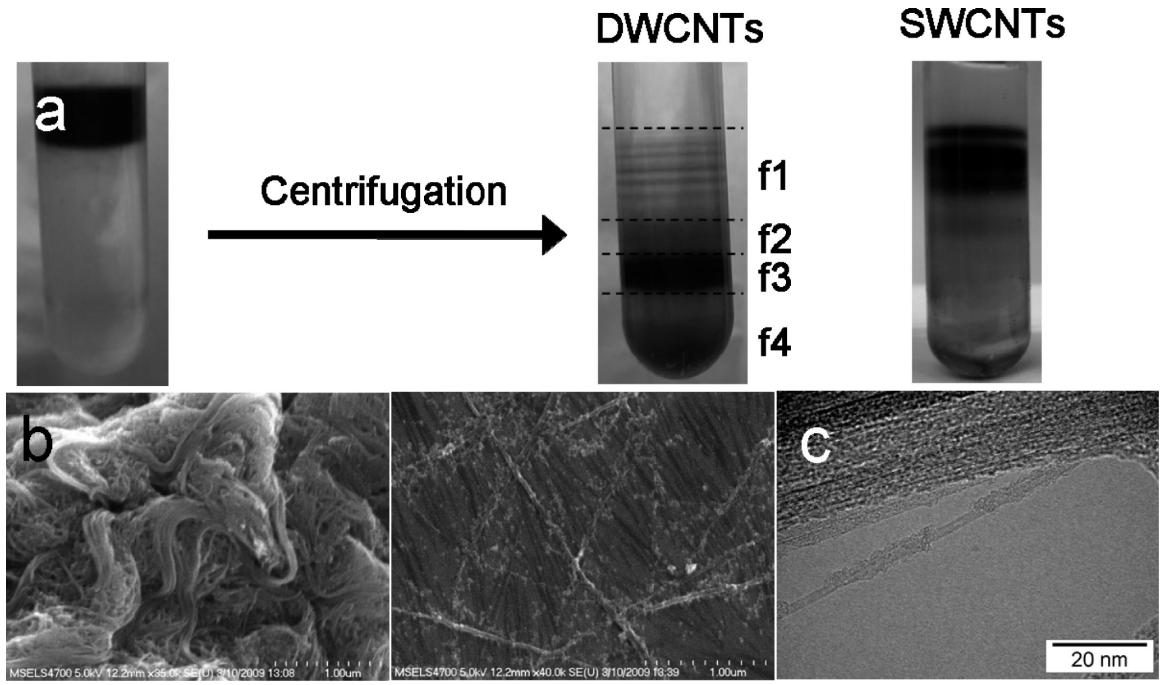

Figure 1. (a) Photograph of a centrifuge tube before (left) and after (right) DGU separation of as-produced DWCNTs. After separation, four sets of bands were obtained, denoted as f1, f2, f3, and f4 from the top. For comparison, photograph of a centrifuge tube after the same DGU separation of electric arc SWCNTs ($d \approx 1.6$ nm) is also shown. (b) SEM images of as-produced DWCNTs (left) and f2 (right) on SiO_2. Surfactant residues are visible in the image of f2. (c) Representative TEM image of fraction 2. The DWCNT is clearly visible. In other images, primarily DWCNTs, but some SWCNTs, were observed.

of the centrifuged supernatant (from the 2 h separation to remove impurities from the sonicated DWCNT suspension) under optimized conditions. Comparable separation results were achieved with DWCNTs synthesized by a chemical vapor deposition (CVD) process (Helix Material Solutions, Inc., Lot # BDCA 07100006) (data not shown). The buoyant density of carbon nanotubes in DGU depends on the overall density of the dispersant encapsulated nanotube, which has contributions from both the structure of the carbon nanotube and the layer of the dispersing agents in aqueous solutions. Due to the higher density of the carbon walls than the overall hydrated surfactant and nanotube structure, DWCNTs encapsulated in DOC surfactant have a greater density than SWCNTs, but a lower density than MWCNTs. This is evident when electric arc SWCNTs with an average diameter ($d \approx 1.6$ nm) similar to that of the DWCNT outer shell were separated under the same conditions. In this case, three sets of bands were obtained near the top of a centrifuge tube, corresponding to different chiralities of SWCNTs, with no measurable concentration of nanotube species apparent below the SWCNT layer (Figure 1a). We note that the first band in the SWCNT sample is likely not SWCNTs, but is more likely C60 size impurities, which are too small to be significantly affected by the applied centrifugation, and pass easily through a 10 000 Da filter.

Given the density differences of SWCNTs, DWCNTs, and MWCNTs in solution, the multiple thin bands of the DWCNT sample in Figure 1a correspond to contaminant SWCNTs in the DWCNT material. This was confirmed by the multiple absorbance peaks (Figure 2a), reminiscent of other HiPco process SWCNTs, and the strong fluorescence intensity (Figure 2b), associated with average diameters in the range of 0.7−1.1 nm.[23] Following ref 1, the second band is thought to contain primarily DWCNTs; the two broad absorbance peaks at 650−860 nm and 900−1300 nm are indicative of energy transitions for DWCNTs with an average external diameter of

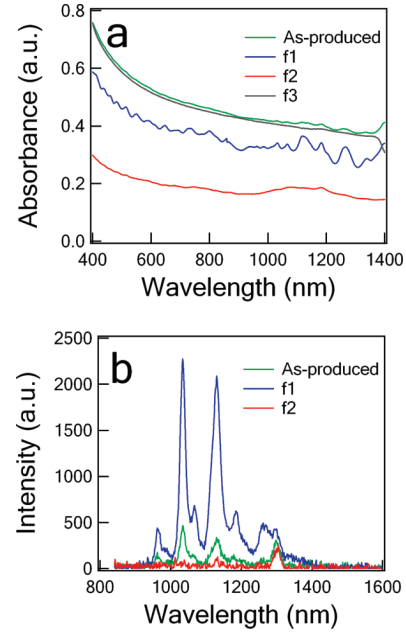

Figure 2. (a) Optical absorbance spectra of layers from a DGU experiment to isolate DWCNTs from contaminate SWCNT components; fraction 2 primarily contains DWCNTs after the separation. (b) Fluorescence spectra at 632 nm excitation of as-produced (green), f1 (blue), and f2 (red) fractions shown in Figure 1a.

~1.6 nm. These could also be indicative of E_{11}^{M} and E_{22}^{S} of large diameter SWCNTs, respectively; however, the shape of the transitions and evidence from ref 1 do not support this interpretation. To support this interpretation, TEM was performed on fraction 2, and primarily DWCNTs, although also some SWCNTs, were noted. A representative image is included in Figure 1C. For the other fractions separated in the centrifugation, the two broad bands on the bottom did not display any measurable absorbance peaks, and are believed to be primarily

MWCNTs and carbonaceous impurities; they were not further studied in this effort.

Focusing on characterization of fraction 2, another method for determining whether the separation was effective is to measure the NIR fluorescence to look for SWCNT contamination. In fractions 2 and higher, the fluorescence intensity at the accessible sub 1610 nm wavelengths was negligible compared to the apparent SWCNT band and the parent dispersion, even though fractions were diluted to the same absorbance at 775 nm as discussed in the Experimental Section (Figure 2b). It should be noted that the peak near 1300 nm arises not from nanotube fluorescence, but is an instrument artifact due to second-order Rayleigh scattering. This is in contrast to the strong fluorescence measured from the apparent SWCNT band, fraction 1, at the same experimental conditions. Consequently, we conclude that the fluorescence detected from the as-produced solution was generated from the SWCNT impurities captured in the top layer after separation. We can thus be reasonably certain that isolated DWCNTs are scanned in the second layer, and not bundled SWCNTs, as some fluorescence would still be expected under the experimental conditions. The absence of fluorescence from the inner walls of DWCNTs is not surprising, as it has previously been reported to be absent in dispersions of HiPco-DWCNTs,[1] peapod-derived DWCNTs,[24] and CVD-DWCNTs.[25] Other reports of fluorescence from the inner DWCNT walls could potentially be related to the presence of incomplete DWCNTs, SWCNT impurities, or large spacing between inner and outer walls in certain synthesized batches.[26] However, fluorescence from the inner walls is demonstrated not to be a fundamental attribute of DWCNT materials.

SEM imaging of the separated DWCNT layer (Figure 1b) confirmed the predominance of nanotubes in the upper layer, and that other impurities had been removed. Additionally, deposition of the DWCNT fraction onto the silicon wafer for SEM imaging was seen not to drive significant bundling of the DWCNTs, either during deposition, or during the subsequent removal of surfactant. However, the separated DWCNT fraction is still observed to be a polydisperse mixture with a distribution of lengths and (because no separation has been applied) wrapping vector pairs. In the remainder of this paper, we discuss the further fractionation of this purified DWCNT population, first by length separation and then by electronic type separation.

Previously, Green et al.[1] reported that solution-dispersed DWCNTs are roughly 44% longer than SWCNTs from the same parent material after DGU processing, and that both length distributions are well described by a log-normal distribution function. Because longer SWCNTs and DWCNTs are expected to display improved material properties, and have been demonstrated to percolate at lower concentrations,[19] even an unfractionated population of DWCNTs is expected to have improved performance in thin film applications in which high electrical conductivity and mechanical resistance are desired. As with SWCNTs,[19] it is likely that fractionation of DWCNTs by length could lead to additionally improved properties for applications. To this end, we separated our separated DWCNT population with respect to length, utilizing an extension of the previously established method for separating SWCNTs that exploits the length-dependent translation of a rod through a dense liquid during centrifugation.[14,15]

The degree and precision of the separation were found to highly dependent on several variables, including separation rate, nanotube concentration, race layer density, and temperature. Centrifugation conditions were extended from the previously optimized condition for SWCNTs,[15,16] with the race layer density

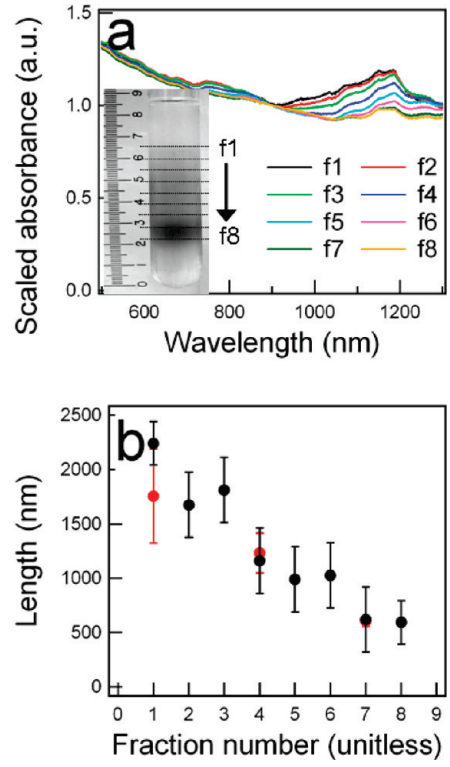

Figure 3. (a) Scaled absorbance spectra of length-sorted DWCNT fractions. Arrow indicates increase in fraction number. The left inset is a photograph of a centrifuge tube after length separation of DWCNTs. The size of the peak features is noted to increase monotonically with length without notable change in the distribution. This is equivalent to the experimental observation of increasing peak to baseline size for SWCNTs.[15] (b) Fraction number versus length measured by DLS (black) and AFM (red). The agreement of the DLS with AFM values is reasonable. Error bars for AFM are the standard deviation of the mean calculated for each fraction.

adjusted to accommodate the higher density of the DWCNTs. The lengths of the fractions were characterized by measuring the correlation function using DLS (Figure 3b) and through AFM (Figure 4). The effective size of the nanotube in the dispersion was previously found to be nearly independent of the nanotube concentration.[15] The top nanotube containing fraction, i.e., containing the nanotube that had moved the farthest from the nanotube injection layer, was found to contain nanotubes with an average length of 2.2 μm. As expected, the average length decreases with increasing fraction number (less distance traveled), as the shorter nanotubes have a greater drag per unit length, and move slowly through the centrifuge tube.[27] Measured average lengths across the fractions decreased from 2.2 to 0.6 μm. AFM measurements reveal that the length distributions within the fractions are relatively narrow (Figure 4), and are in good agreement with the DLS results. To account for the variations of nanotube concentration in the collected fraction, the optical absorbance spectra were scaled at 900 nm, a wavelength with minimal apparent excitonic optical transitions. As discussed previously, scaling of the absorbance spectra did not change the order of magnitude of the observed length dependence, regardless of the scaling location chosen.[17] Figure 3a shows that the optical absorbance increases as the fraction number decreases, corresponding to the longer nanotubes, which is consistent with recent work by Fagan et al.[14,15] Comparison of the increase in DWCNT absorbance intensity with the approximately linear dependence on the nanotube length measured for SWCNTs reveals that the slope of the increase is approximately 1/3 to 1/2 the value expected for dispersions with

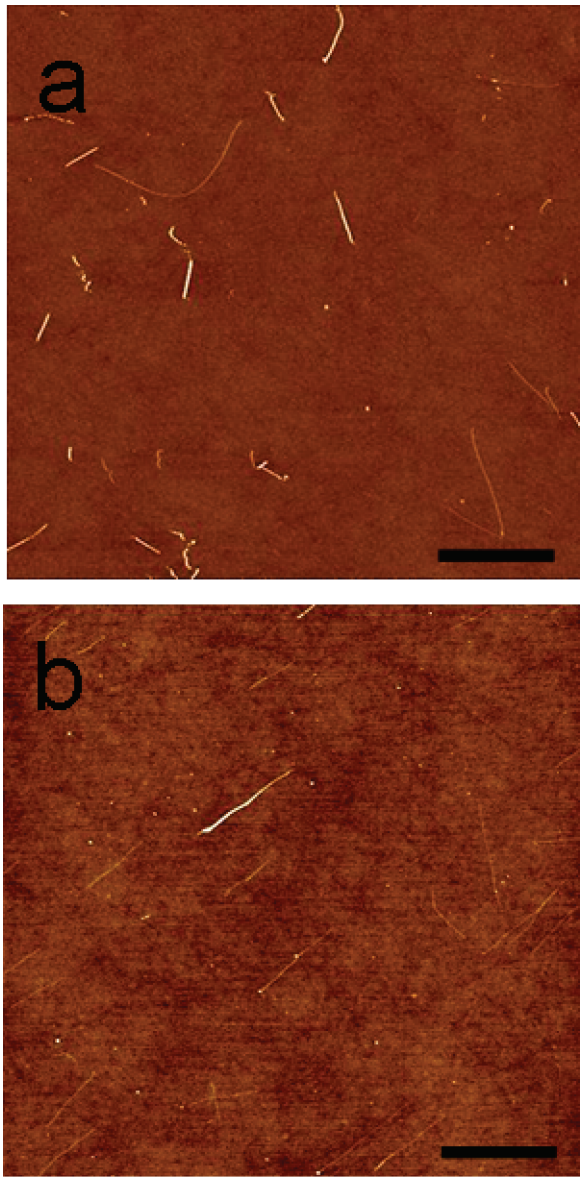

Figure 4. AFM images on SiO_2 with an APTES SAM of (a) unsorted and (b) f4 of the length-separated DWCNT fractions from Figure 3a. The average length for f4 was determined as 1.23 ± 0.18 μm, which is in reasonable agreement with the DLS value, 1.16 ± 0.3 μm, in Figure 3b.

mixtures of large and small diameter SWCNTs. It is unclear whether this difference is due to the longer average lengths of the DWCNTs (the trend for SWCNTs trails off at a length scale around 1 μm), or to interactions between the walls of the DWCNTs. Trends in the DWCNT absorbance are also less quantitative compared to those previously measured for SWCNTs,[14−16] due to the difficulty in finding a local minimum between the broader absorbance peak features and the smaller relative feature size (compared to the π plasmon background) expected from the increase in carbon mass per unit length in DWCNTs. There were no measurable shifts with increasing length in the energy of the optical transitions.

Separation by electronic type is particularly interesting due to potential thin film applications. Recently, we have replicated the separation of metallic from semiconducting SWCNTs[8,9] for both laser ablation ($d \approx 1.4$ nm) and electric arc discharge ($d \approx 1.6$ nm) synthesis techniques using DGU through the controlled addition of SDS and SC as cosurfactants. In both cases, the upper layers after the DGU process are enriched in metallic-type SWCNTs, with the semiconducting SWCNTs remaining in a lower band (data not shown). As the intrinsic density of metallic SWCNTs has been found to be similar to that of semiconducting SWCNTs when dispersed in the same surfactant solution,[8,28] the density difference exploited for the metallic from semiconducting separation is hypothesized to depend on the different binding properties of the cosurfactants. However, other theories have also been advanced in the literature.[36] Since the outer walls of DWCNTs studied in this work have similar diameters to those of laser ablation and electric arc SWCNTs, the separation of DWCNTs was attempted under similar conditions, described previously. After centrifugation, we obtained two bands on the top (fractions 1 and 2) and two bands on the bottom (fractions 3 and 4) (Figure 5a). By comparison to the separation achieved for large diameter SWCNTs, we initially suspected that the outer walls of fractions 1−2 and 3−4 are primarily metallic and semiconducting, respectively. The SEM images exhibited long rod-like shapes in both fractions 1 and 3 (Figure 5c). In Figure 5b, fractions 2, 3, and 4 show sharp absorbance peaks at 900−1300 nm and 1600−2000 nm, corresponding to the semiconducting interband transition, a combination of E^S_{11} of inner wall and E^S_{22} of outer wall at the shorter wavelength and E^S_{11} of outer wall in the (1600 to 2000) nm range. Above 2000 nm, the absorbance spectra lose accuracy due to the strong absorbance of water in this region. In contrast, both semiconducting absorbance peaks were significantly reduced in fraction 1. This provides strong evidence that this band is distinguishable from others. Thus the uppermost band (fraction 1) was hypothesized to consist of predominantly metallic nanotubes, whereas the lower bands (fractions 3 and 4) would be enriched in semiconducting nanotubes (Figure 5b). Both the inner and outer walls, however, contribute the absorbance spectra of DWCNTs, limiting the interpretation. For instance, for the anticipated diameter of the inner and outer walls, the E^S_{22} of the outer walls overlaps the E^S_{11} of the inner walls.

In order to gain further insight into the electronic properties of the separated fractions, resonant Raman scattering was performed, allowing for a reliable characterization of individual nanotubes. The RBM corresponds to symmetric in-phase displacements of all the carbon atoms in the nanotube in the radial direction, which distinguishes a nanotube from other types of carbon materials.[6] The RBM frequency depends on the nanotube diameter in a manner inversely proportional to the number of carbon atoms on the circumference of the nanotube.[6] Three different excitation wavelengths, 514.5, 632, and 785 nm, corresponding to 2.41, 1.96, and 1.58 eV were initially chosen, and the inner walls were detected to be in resonance at 785 nm (1.58 eV), as shown in Figure 6. In Figure 6, both lower (<200 cm^{-1}) and higher frequency (>200 cm^{-1}) RBM features are observed. All samples were dialyzed to remove iodixanol prior to measurement; the DOC surfactant does not contribute a Raman signal in this region. Given the relation ω_{RBM} (cm^{-1}) = 227/d (nm),[29] these different frequency regions appear to originate from the outer and inner walls, respectively. Using the relation for the RBM frequency, the average diameters of inner and outer walls probed in Figure 6 were estimated as 0.8 to 1.1 nm and as approximately 1.4 nm, respectively. We note that, for larger diameter nanotubes (d > 1.4 nm), nonuniversal relations between the RBM frequency and the inverse nanotube diameter have been proposed,[30] which limits the use of the RBM frequency for the study of MWCNTs.

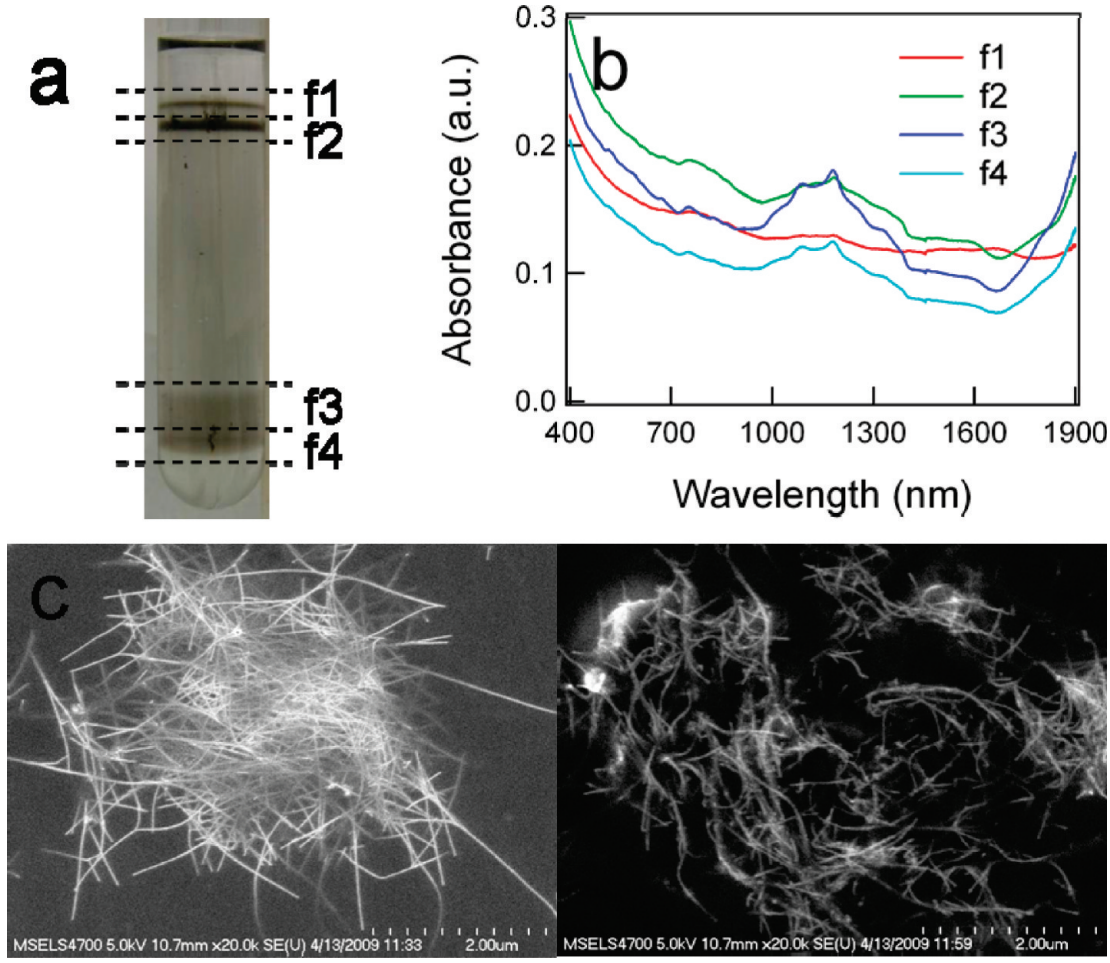

Figure 5. (a) Photograph of a centrifuge tube after separation of purified DWCNTs by electronic structure using the controlled addition of cosurfactants. After separation, four sets of bands were obtained, denoted as f1, f2, f3, and f4 from the top. (b) Optical absorbance spectra of f1 (red), f2 (green), f3 (blue), and f4 (light blue). Strong optical transitions corresponding to semiconducting chiralities are noted in f3 and f4. The first-order semiconducting interband transition peak, E_{11}^{S} of the outer wall is visible at the edge of the wavelength range. (c) SEM images of f1 (left) and f3 (right) on SiO_2. The images demonstrate that it is nanotubes being separated in the procedure, and not a removal of an impurity material.

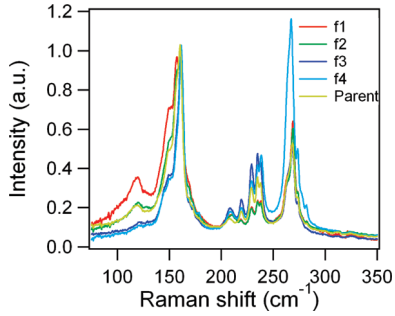

Figure 6. Scaled Raman spectra of RBM features taken from the separated f1 (red), f2 (green), f3 (blue), and f4 (light blue) in Figure 5a, and unsorted parent DWCNT solution (dark yellow). All fractions were dialyzed to remove iodixanol prior to the Raman measurement. The measured RBM spectra have been scaled at 195 cm^{-1} to account for the differences of DWCNT concentration in the collected fraction. Note that the parent fraction is intermediate to the two pairs of f1,f2 and f3,f4; this distribution is consistent with partial separation of the metallic and semiconducting chirality shells in resonance at 785 nm.

Because the measured RBM mode scattering in SWCNTs and DWCNTs is primarily due to electronic resonance-enhanced Raman scattering, the combination of observed frequencies and excitation energies can be used to make general identification of the observed nanotube electronic type through the use of a Kataura plot.[31] Variations of nanotube concentration in the collected fraction were considered by scaling the Raman spectra at a nonpeak location, 195 cm^{-1}. Relative intensity in the Raman spectra was then correlated to selective enrichment or depletion of specific species. According to the revised Kataura plot,[32] which was experimentally compiled using spectrofluorimetry and Raman excitation profiles to map the interband transitions for semiconductors and metals, respectively, the RBM peaks near 235 cm^{-1} are attributed to the semiconducting inner walls. We note that scaled RBM intensity of fraction 1 in this region is significantly lower than that in other fractions, indicating depletion of semiconducting inner walls. In contrast, fraction 1 was enriched in RBM modes, indicative of metallic-type inner walls. Reassuringly, the scaled RBM intensity of the unsorted, parent solution was in between fractions 1 and 2 and fractions 3 and 4, suggesting fractionation toward the top of the centrifuge tube of DWCNTs with metallic inner walls, and fractionation toward the bottom of those with semiconducting inner walls. Unfortunately, too few resonant outer walls were measurable at the selected excitation wavelengths to make conclusive statements regarding their electronic characteristics.

Thin films of selected metallic-enriched DWCNTs (fraction 1 in Figure 5a) and semiconducting-enriched DWCNTs (fraction 3 in Figure 5a) represent distinctly different optical and electrical properties (Figure 7). Figure 7a shows the transmittance spectra of thin films of DWCNT fractions 1 and 3 with the average tube length of 1 μm and surface concentration of 1 $\mu g/cm^2$. These DWCNTs exist above the critical percolation concentra-

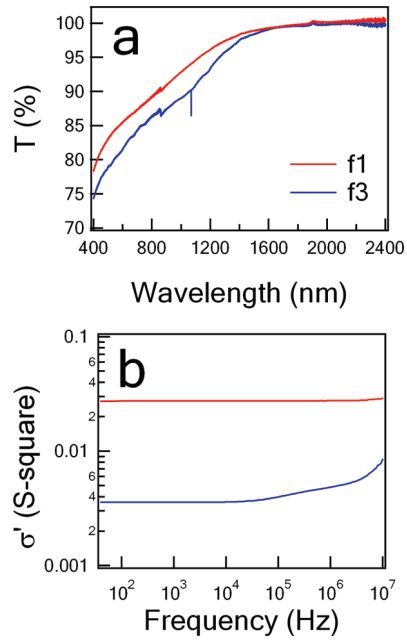

Figure 7. (a) Optical transmittance and (b) sheet conductivity σ' of metal-enriched DWCNTs f1 (red) and semiconductor-enriched DWCNTs f3 (blue) in Figure 5a.

tion, 0.1 μg/cm^2,[19] measured for SWCNTs, and are almost certainly in a percolated network with a thickness of 20−30 nm. In the case of the film consisting of fraction 3, the broad absorption band appears near 1100 nm, attributed to the semiconducting electronic transition, similar to that of liquid suspension in Figure 5b. In contrast, the film containing metal-enriched DWCNTs (fraction 1) show a gradual decrease in transmittance at wavelengths shorter than 1200 nm. The electronic transitions arising from both semiconducting and metallic chiralities are not clearly visible in Figure 7. The film transmittance at 770 nm is ~90% for both fractions 1 and 3, while the metal-enriched fraction 1 is more transparent in the visible range. For the corresponding fractions, the normalized absorption intensity of the films is lower than that of the liquid suspensions in Figure 5b. The decrease in intensity of the characteristic electronic transitions can be attributed to interactions between interconnecting tubes,[33] or doping by oxygen from the ambient atmosphere. This effect should be present in our films where the protective surfactant coating has been washed away. The metallic transition is likely to be affected more strongly than the semiconducting transition,[19] which accounts for the higher transparency of metal-enriched DWCNTs.

We note that a thin film consisting of fraction 1 was an order of magnitude more conductive than a film composed of fraction 3 at similar concentrations (Figure 7b). The surface conductance σ' of the percolated network of fraction 1 was 0.027 S-square, independent of frequency up to 10 MHz. On the basis of the high transparency (Figure 7a), the network of metal-enriched DWCNTs is attractive for transparent conductors. In contrast, the surface conductance of fraction 3 is 0.0035 S-square at zero frequency, and it exhibits a plateau up to a crossover frequency ω_s of 10 kHz. At higher frequencies, $\omega > \omega_s$, we observe that σ' increases with increasing frequency according to power law $\sigma' \sim \omega^n$, which is commonly described as a "universal" property of disordered solids, and applicable to a broad range of semiconducting materials, conductor-dielectric mixtures, and composites.[34,35] These observations indicate that considerable control of the conductance and optical properties can be obtained by adjusting the tube length and type.

Conclusion

We have separated as-produced nanotubes by the number of walls using the difference in buoyant density, leading to SWCNTs, DWCNTs, and MWCNTs. DWCNTs were separated by length, with fractions ranging from 0.6 to 2.2 μm in average length resolved. AFM measurements on individual DWCNTs revealed narrow length distribution in the separated fractions. The intrinsic optical response of DWCNTs was found to increase with their length, consistent with SWCNTs, however, at a lesser rate than expected for a mixture of SWCNTs with diameters similar to the inner and outer walls of the DWCNTs. On the basis of the improved properties and reduced percolation threshold with an increase in aspect ratio, longer nanotube materials, including DWCNTs, are expected to display better performance in many applications of carbon nanotubes. In addition, the enrichment or depletion of specific electronic structure in DWCNTs was achieved based on the organization of surfactants on nanotubes of different electronic nature. Analysis of UV−vis−NIR optical absorbance, resonant Raman spectra (RBM modes), and electrical conductivity measurements confirmed that this separation provides metal-enriched DWCNTs on the top and semiconductor-enriched DWCNTs on the bottom after centrifugation. This result has substantial implication for various applications of DWCNTs. For instance, metallic DWCNTs could be useful for coaxial cables or capacitors, and semiconducting DWCNTs are well suited for applications such as field emission transistors and sensors. Further characterization of the electronic structure or chirality enrichment of the DWCNTs is underway. It should be noted that iteration of the DGU process and adjusting the relative concentration of surfactants would likely improve the resolution of the various species.

Acknowledgment. The authors thank E. K. Hobbie and M. Zheng for useful discussions. This work is an official contribution of the National Institute of Standards and Technology and is not subject to copyright in the United States.

References and Notes

(1) Green, A. A.; Hersam, M. C. *Nat. Nanotechnol.* **2008**, *264*, 1.
(2) Pfeiffer, R.; Simon, F.; Kuzmany, H.; Popov, V. N. *Phys. Rev. B* **2005**, *72*, 161404.
(3) Shimada, T.; Sugai, T.; Ohno, Y.; Kishimoto, S.; Mizutani, T.; Yoshida, H.; Okazaki, T.; Shinohara, H. *Appl. Phys. Lett.* **2004**, *84*, 2412.
(4) Li, Y. F.; Hakakeyama, R.; Kaneko, T.; Izumida, T.; Okada, T.; Kato, T. *Appl. Phys. Lett.* **2006**, *89*, 093110.
(5) Ha, B.; Shin, D. H.; Park, J.; Lee, C. J. *J. Phys. Chem. C* **2008**, *112*, 430.
(6) Saito, R.; Matsuo, R.; Kimura, T.; Dresselhaus, G.; Dresselhaus, M. S. *Chem. Phys. Lett.* **2001**, *348*, 187.
(7) Saito, R.; Dresselhaus, G.; Dresselhaus, M. S. *Physical Properties of Carbon Nanotubes*; Imperial College Press: London, 1998.
(8) Arnold, M. S.; Green, A. A.; Hulvat, J. F.; Stupp, S. I.; Hersam, M. C. *Nat. Nanotechnol.* **2006**, *1*, 60.
(9) Yanagi, K.; Miyata, Y.; Kataura, H. *Appl. Phys. Express* **2008**, *1*, 034003.
(10) Hayashi, T.; Shimamoto, D.; Kim, Y. A.; Muramatsu, H.; Okino, F.; Touhara, H.; Shimada, T.; Miyauchi, Y.; Maruyama, S.; Terrones, M.; Dresselhaus, M. S.; Endo, M. *ACS Nano* **2008**, *2*, 485.
(11) Dresselhaus, M. S.; Dresselhaus, G.; Hofmann, M. *J. Vac. Sci. Technol., B* **2008**, *26*, 1613.
(12) Heller, D. A.; Mayrhofer, R. M.; Baik, S.; Grinkova, Y. V.; Usrey, M. L.; Strano, M. S. *J. Am. Chem. Soc.* **2006**, *126*, 14567.
(13) Huang, X.; Mclean, R. S.; Zheng, M. *Anal. Chem.* **2005**, *77*, 6225.
(14) Bauer, B. J.; Becker, M. L.; Bajpai, V.; Fagan, J. A.; Hobbie, E. K.; Migler, K. B.; Guttman, C. M.; Blair, W. R. *J. Phys. Chem. C* **2007**, *111*, 17914.
(15) Fagan, J. A.; Becker, M. L.; Chun, J.; Nie, P.; Bauer, B. J.; Simpson, J. R.; Hight Walker, A. R.; Hobbie, E. K. *Langmuir* **2008**, *24*, 13880.
(16) Fagan, J. A.; Becker, M. L.; Chun, J.; Hobbie, E. K. *Adv. Mater.* **2008**, *20*, 1609.

(17) Fagan, J. A.; Simpson, J. R.; Bauer, B. J.; De Paoli Lacerda, S. H.; Becker, M. L.; Chun, J.; Migler, K. B.; Hight Walker, A. R.; Hobbie, E. K. *J. Am. Chem. Soc.* **2007**, *129*, 10607.

(18) Becker, M. L.; Fagan, J. A.; Gallant, N. D.; Bauer, B. J.; Bajpai, V.; Hobbie, E. K.; Lacerda, S. H.; Migler, K. B.; Jakupciak, J. P. *Adv. Mater.* **2007**, *19*, 939.

(19) Simien, D.; Fagan, J. A.; Luo, W.; Douglas, J. F.; Migler, K. B.; Obrzut, J. *ACS Nano* **2008**, *2*, 1879.

(20) Doi, M.; Edwards, S. F. *The Theory of Polymer Dynamics*; Oxford Science Publications, New York, 1986.

(21) Pecora, R. *Annu. Rev. Biophys. Bioeng.* **1972**, *1*, 257.

(22) Wu, Z.; Chen, Z.; Du, X.; Logan, J. M.; Sippel, J.; Nikolou, M.; Kamaras, K.; Reynolds, J. R.; Tanner, D. B.; Hebard, A. F.; Rinzler, A. G. *Science* **2004**, *305*, 1273.

(23) Weisman, R. B.; Bachilo, S. M. *Nano Lett.* **2003**, *3*, 1235.

(24) Okazaki, T.; Bandow, S.; Tamura, G.; Fujita, Y.; Iakoubovskii, K.; Kazaoui, S.; Minami, N.; Saito, T.; Suenaga, K.; Iijima, S. *Phys. Rev. B* **2006**, *74*, 153404.

(25) Iakoubovskii, K.; Minami, N.; Ueno, T.; Kazaoui, S.; Kataura, H. *J. Phys. Chem. C* **2008**, *112*, 11194.

(26) Tsyboulski, D. A.; Hou, Y.; Fakhri, N.; Ghosh, S.; Zhang, R.; Bachilo, S. M.; Pasquali, M.; Chen, L.; Liu, J.; Weisman, B. R. *Nano Lett.* **2009**, *9*, 3282.

(27) Batchelor, G. K. *J. Fluid Mech.* **1970**, *44*, 419.

(28) Yanagi, K.; Iitsuka, T.; Fujii, S.; Kataura, H. *J. Phys. Chem. C* **2008**, *112*, 18889.

(29) Jorio, A.; Fantini, C.; Pimenta, M. A.; Capaz, R. B.; Samsonidze, Ge. G.; Dresselhaus, G.; Dresselhaus, M. S.; Jiang, J.; Kobayashi, N.; Grüneis, A.; Saito, R. *Phys. Rev. B* **2005**, *71*, 075401.

(30) Dresselhaus, M. S.; Dresselhaus, G.; Jorio, A. *J. Phys. Chem. C* **2007**, *111*, 17887.

(31) Kataura, H.; Kumazawa, Y.; Maniwa, Y.; Umczu, I.; Suzuki, S.; Ohtsuka, Y.; Achiba, Y. *Synth. Met.* **1999**, *103*, 2555.

(32) Strano, M. S. *J. Am. Chem. Soc.* **2003**, *125*, 16148.

(33) Fuhrer, M. S.; Nygard, J.; Shioh, L.; Forero, M.; Yoon, Y. G.; Mazzoni, M. S. C.; Choi, H. J.; Louie, S. G.; Zeth, A.; McEuen, P. L. *Science* **2000**, *288*, 494.

(34) Obrzut, J.; Page, A. K. *Phys. Rev. B* **2009**, *80*, 195211.

(35) Obrzut, J.; Douglas, J. F. *Metrol. Meas. Syst.* **2009**, *14*, 399.

(36) Carvalho, E. J. F.; dos Santos, M. C. *ACS Nano* **2010**, *4*, 765.

(37) Endo, M.; Muramatsu, H.; Hayashi, T.; Kim, Y. A.; Terrones, M.; Dresselhaus, M. S. *Nature* **2005**, *433*, 476.

(38) Kim, Y. A.; Muramatsu, H.; Hayashi, T.; Endo, M.; Terrones, M.; Dresselhaus, M. S. *Chem. Phys. Lett.* **2004**, *398*, 87.

(39) Hashimoto, A.; Suenaga, K.; Urita, K.; Shimada, T.; Sugai, T.; Bandow, S.; Shinohara, H.; Ijima, S. *Phys. Rev. Lett.* **2005**, *94*, 045504.

(40) Yamada, T.; Namai, T.; Hata, K.; Futaba, N. D.; Mizuno, K.; Fan, J.; Yudasaka, M.; Yumura, M.; Iijima, S. *Nature* **2006**, *1*, 131.

(41) Kuwahara, S.; Akita, S.; Shirakihara, M.; Sugai, T.; Nakayama, Y.; Shinohara, H. *Chem. Phys. Lett.* **2006**, *429*, 581.

(42) Hertel, T.; Hagen, A.; Talalaev, V.; Arnold, K.; Hennrich, F.; Kappes, M.; Rosenthal, S.; McBride, J.; Ulbricht, H.; Flahaut, E. *Nano Lett.* **2005**, *5*, 511.

(43) Lovall, D.; Buss, M.; Graugnard, E.; Andres, R. P.; Reifenberger, R. *Phys. Rev. B* **2000**, *61*, 5683.

(44) Kociak, M.; Suenage, K.; Hirahara, K.; Saito, Y.; Nakahira, T.; Ijiima, S. *Phys. Rev. Lett.* **2002**, *89*, 155501.

(45) Chen, G.; Bandow, S.; Margine, E. R.; Nisoli, C.; Kolmogorov, A. N.; Crespi, V. H.; Gupta, R.; Sumanasekera, G. U.; Eklund, P. C. *Phys. Rev. Lett.* **2003**, *90*, 257403.

(46) Legoas, S. B.; Coluci, V. R.; Braga, S. F.; Coura, P. Z.; Dantas, S. O.; Galvao, D. S. *Phys. Rev. Lett.* **2003**, *90*, 05504.

(47) Liang, S. D. *Physica B* **2004**, *352*, 305.

(48) Song, W.; Ni, M.; Lu, J.; Gao, Z.; Nagase, S.; Yu, D.; Ye, H.; Zhang, X. *Chem. Phys. Lett.* **2005**, *414*, 429.

(49) Certain equipment, instruments, or materials are identified in this paper in order to adequately specify the experimental details. Such identification does not imply recommendation by the National Institute of Standards and Technology nor does it imply the materials are necessarily the best available for the purpose.

JP9110376